RSC Advances

PAPER

View Article Online
View Journal | View Issue

Cite this: *RSC Adv.*, 2024, **14**, 18064

Synthesis of graphitic carbon nitride-based nanocomposites and their mechanical properties in epoxy compositions

Sugyeong Jeon,†[ab] Hye Jin Kim,†[a] Hyeon-Gook Kim,[a] Meysam Tayebi,[a] Seoyoon Yu,[a] Jong-Hyun Kim,[a] Bongkuk Seo,[a] Choongsun Lim *[a] and Weon Bae Ko*[b]

Received 9th April 2024
Accepted 15th May 2024

DOI: 10.1039/d4ra02670e

rsc.li/rsc-advances

Thermoset epoxy resins are widely used in research and commercial applications. Zeolite imidazole framework-8 (ZIF-8), graphitic carbon nitride (GCN, g-C_3N_4), and S-doped graphitic carbon nitride (SCN, S-g-C_3N_4) composites were synthesized as accelerators and their effects on the physical properties of epoxies were examined. An ultrasound-assisted method was used to prepare ZIF-8/GCN and ZIF-8/SCN nanocomposites while g-C_3N_4 and S-g-C_3N_4 were prepared from the calcination of melamine and thiourea, respectively. The surface morphology, and particle size were characterized by scanning electron microscopy, and X-ray diffraction. The properties of synthesized nanocomposites were measured using Fourier-transform infrared spectroscopy. After the accelerator was added to the epoxy composites, their activation energies were calculated using differential scanning calorimetry. The tensile strength and flexural strength were measured using a universal testing machine and impact strength was measured by using an Izod impact strength tester. The impact strength of ZIF-8/SCN nanocomposites was enhanced by 45.2%. The storage stability of the epoxy compositions with different catalysts was evaluated by measuring the variation of viscosity with time at a constant temperature.

Introduction

Epoxy resins are the most widely used thermosets in industry, such as surface coatings, structural adhesives, and molding composites, because of their high chemical and creep resistances.[1–3] Polymerization of epoxy resin requires a curing agent and reaction promoter.[4] While several latent curing agents, such as dicyandiamide (DICY), diaminodiphenyl sulfone (DDS), or polyamide, are available for one-pot epoxy systems, DICY is the most commonly used. However, its melting point (190 °C) is close to the curing temperature of epoxy resins, causing its poor solubility in them.[5] Epoxy resins can be cured at low temperatures by adding promoters, such as tertiary amines, imidazole, and urea.[6–10] Amine curing agents can induce anionic polymerization in the glycidyl ether of epoxy resins.[11]

Zeolitic imidazolate framework-8 (ZIF-8) composed of Zn^{2+} ions and 2-methylimidazole (2-MI) ligands has been shown to act as an accelerator for epoxy polymerizations and it has high storage stability.[12] ZIF-8 has high porosity, large surface area, and exhibits high thermal and chemical stability in compositions that easily form strong interactions with polymers, resulting in cured epoxies with enhanced physical properties.[13]

In this study, ZIF-8/graphitic carbon nitride (GCN) and ZIF-8/S-doped graphitic carbon nitride (SCN) nanocomposites with enhanced mechanical properties were synthesized for use as curing reaction accelerators as well as physical properties modifiers. GCN nanosheets are 2D sheets composed of interconnected secondary nitrogen tri-*s*-triazines[14] that have a facile method of synthesis, an attractive electronic band structure, high physicochemical stability, and are abundant on Earth.[15] The high thermal and chemical stabilities of GCN are attributed mainly to its π-conjugated stacked structure that is composed of repeated tri-*s*-triazine units with van der Waals forces between the layered sheets.[16] GCN can be prepared *via* thermal condensation using various types of raw materials comprising heptazine units, including melamine, cyanamide, dicyandiamide, thiourea, urea, and their mixtures.[17] GCN has been widely used in catalysts,[18,19] hydrogen devices,[20] lithium-ion storage,[21] and optoelectronic equipment.[22] Wang *et al.* revealed that the tensile and flexural moduli of GCN/epoxy nanocomposites increased by 32% and 28%, respectively.[23] Shi *et al.* discovered that adding 6.0 wt% GCN to sodium alginate (SA) nanocomposite films dramatically increased their tensile strength by 103%.[24] Qi *et al.* discovered that in GCN/epoxy composites, GCN formed amide reaction sites or hydrogen bonds with the epoxy

[a]*Research Center for Advanced Specialty Chemicals, Korea Research Institute of Chemical Technology, Ulsan, Republic of Korea. E-mail: chsunlim@krict.re.kr*

[b]*Department of Convergence Science, Graduate School, Sahmyook University, Seoul, Republic of Korea. E-mail: kowb@syu.ac.kr*

† Sugyeong Jeon, and Hye Jin Kim are equally contributed for the research.

matrix, exhibiting improved thermal properties.[25] Furthermore, SCN having sulfur on the surface of two dimensional sheet of graphitic carbon nitride has potential constructing more rigid structure due to S=C bonds rather than N=C bonds of GCN.

The synthesized both GCN and SCN nanocomposites were formulated with epoxy to measure changes in the mechanical properties of the epoxy compositions, respectively. These epoxy compositions were investigated using a rotatory viscoelastic analyzer and time-dependent changes in viscosity and their activation energies were measured using differential scanning calorimetry (DSC).

Experimental

Zinc acetate dihydrate ($(Zn(CH_3COO)_2 \cdot 2H_2O)$) was purchased from Alfa Aesar (Korea). 20 methylimidazole (2-MI; $CH_2C_3H_3N_2$) and poly(vinyl)pyrrolidone (PVP; $(C_6H_9NO)_n$; average mol wt. 10 000), melamine ($C_3H_6N_6$), and thiourea (NH_2CSNH_2) were obtained from Sigma-Aldrich (Korea). Methanol and isopropyl alcohol (IPA) were purchased from Samchun (Republic of Korea), diglycidyl ether of bisphenol A (DGEBA; Epikote 828) was purchased from Momentive Performance Materials Korea Co. Ltd, and DICY was purchased from Airproducts and Chemicals (USA).

Synthesis of ZIF-8

$Zn(CH_3COO)_2 \cdot 2H_2O$ (0.295 g) and PVP (0.1 g) were dissolved in methanol (25 mL) and stirred for 30 min. Afterward, 25 mL of a methanol solution of 2-MI (0.66 g) was added to the solution and subsequently stirred for 2 h at room temperature. The precipitate was washed several times with methanol and the sample was collected after centrifuging.

Synthesis of ZIF-8/GCN and ZIF-8/SCN nanocomposites

GCN and SCN were synthesized from the calcination of melamine and thiourea, respectively.[26] The precursors (10 g) were poured into an alumina crucible, the temperature was raised to 550 °C at 5 °C min^{-1}, and maintained for 2 h (melamine) or 5 h (thiourea) in the furnace. After cooling to room temperature, the resulting yellow powder was reheated under the same conditions and subsequently dispersed in IPA by sonication.

The synthesized GCN or SCN (20 mg) was dispersed in 25 mL of methanol by sonication, and $Zn(CH_3COO)_2 \cdot 2H_2O$ (0.295 g) and PVP (0.1 g) were subsequently added to the solution. The solution was sonicated for 30 min, 25 mL methanol solution of 2-MI was added, and it was subsequently stirred for 2 h at room temperature. The precipitate was washed several times with methanol and ZIF-8/GCN and ZIF-8/SCN nanocomposites were collected after centrifuging.

Preparation of test specimens

The epoxy curing system was prepared by mixing DGEBA, DICY, and a reaction accelerator, such as 2-MI, ZIF-8, ZIF-8/GCN, or ZIF-8/SCN nanocomposites. Regarding the paste, the equivalent ratio between the epoxy resin (DGEBA) and DICY was 1 : 0.9 (Table 1). The components were mixed and stirred using a planetary paste mixer at 2000 rpm for 40 min and degassed at 2200 rpm for 20 min. The prepared compositions were poured into a metal mold and cured at 150 °C for 0.5 h and subsequently at 170 °C for 1.5 h, 180 °C for 1 h to provide the mechanical test specimens.

Table 1 Formulation of the epoxy compositions

	DGEBA (g)	DICY	2-MI	ZIF-8	ZIF-8/GCN	ZIF-8/SCN
2-MI	100	11.24	0.21			
ZIF-8	100	11.24		0.21		
ZIF-8/GCN	100	11.24			0.21	
ZIF-8/SCN	100	11.24				0.21

Instrumental methods

Crystal structures and average crystallite sizes of the samples were analyzed using powder X-ray diffraction (XRD; Ultima IV, Rigaku, Japan) with a Cu Kα radiation source ($\lambda = 1.541$ nm) by scanning within a 2θ range of 5–50°. Fourier-transform infrared spectroscopy (FTIR; Thermo Fisher Scientific Nicolet Continuum IR Microscope) was used to obtain information on the functional groups in the samples. The morphology of the accelerator was observed using field-emission scanning electron microscopy (FE-SEM; EDS, TESCAN MIRA 3, Kohoutovice, Czech Republic) at an acceleration voltage of 15 kV. The vibrational state of the sample was investigated using Raman spectroscopy at a wavelength of 780 nm (DXR, Thermo Fisher Scientific, USA). The viscoelastic behavior of the cured epoxy compositions was studied using dynamic mechanical analysis (DMA; Q800, TA Instruments, DE, USA) at an amplitude of 10 μm and a heating rate of 5 °C min^{-1} from 25 to 200 °C on test specimens having dimensions of 60 mm × 12 mm × 3 mm. The coefficients of thermal linear expansion (CTE) of the cured epoxy polymers were measured using thermomechanical analysis (TMA; Q400, TA Instruments, DE, USA) performed at a heating rate of 2 °C min^{-1} in the 25–250 °C range on test specimens with dimensions of 5 mm × 5 mm × 3 mm. Kinetic studies of the epoxy compositions with the promoters were performed in N_2 using DSC (TA Instruments Q-200, DE, USA) in the temperature range of 80 to 250 °C and heating rates of 2, 5, 10, and 20 °C min^{-1} to obtain the activation energy of the reaction. The tensile and flexural strengths of the epoxy compositions were measured using a universal testing machine (UTM 5982, Instron, MA, USA) following ASTM D638 and ASTM D7264M methods. The impact strength of the epoxy compositions was measured using an Izod impact-testing machine. A rotatory viscoelastic analyzer (HR 20, TA Instruments, USA) was used to measure the viscosity of the epoxy compositions at 40 °C and 60 °C.

Results and discussions

The XRD patterns of ZIF-8/GCN and ZIF-8/SCN nanocomposites are shown in Fig. 1. Characteristic ZIF-8 and GCN peaks are observed in the ZIF-8/GCN and ZIF-8/SCN nanocomposites.

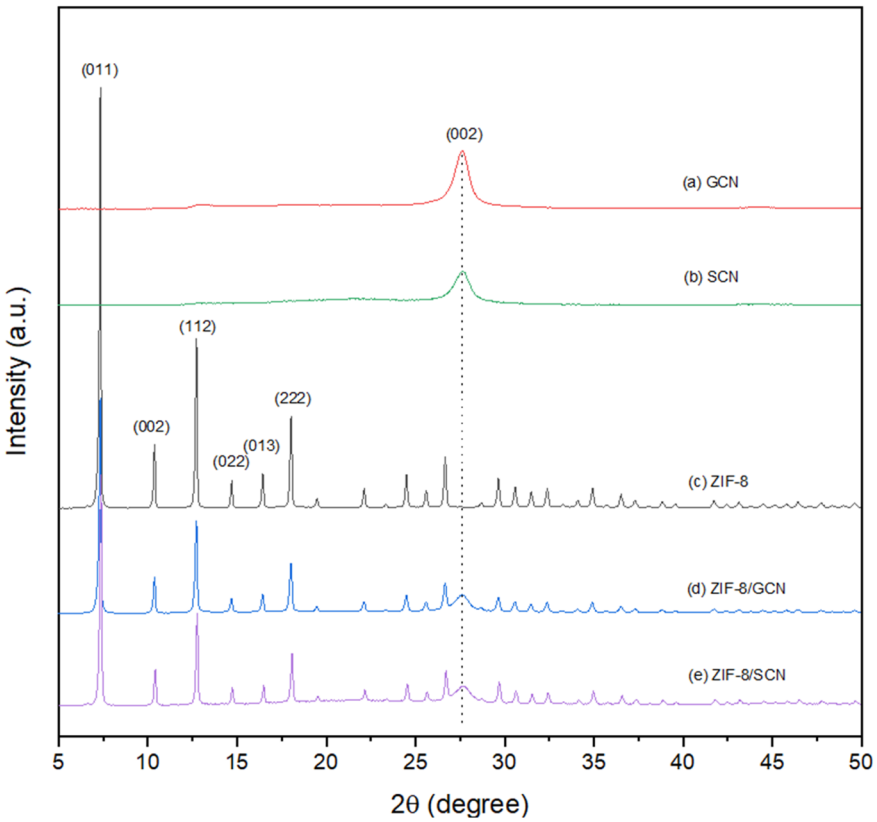

Fig. 1 XRD patterns of synthesized (a) GCN, (b) SCN, (c) ZIF-8, (d) ZIF-8/GCN, and (e) ZIF-8/SCN.

Regarding ZIF-8, the XRD peaks observed at $2\theta = 7.34°$, 10.36°, 12.70°, 14.71°, 16.45°, and 18.03° correspond to the (011), (002), (112), (022), (013), and (222) planes of the sodalite structure (JCPDS 00-062-1030), respectively. The XRD pattern in Fig. 1 shows a GCN peak observed at $2\theta = 27.60°$, which corresponds to the (002) plane (JCPDS 87-1526).[27] The SCN peak is widened and weakened, which could be due to lattice distortion and the small size effect after S doping in the GCN framework. The 0.1% of atomic ratio of S in SCN was confirmed by elemental analysis.[28]

The FT-IR spectra of ZIF-8/GCN and ZIF-8/SCN nanocomposites in Fig. 2 show the major peaks of ZIF-8 and the prominent modes of GCN and SCN in the wavelength range of 400–4000 cm^{-1}. The absorption bands at 1200 and 1700 cm^{-1} are attributed to the vibrational modes of CN heterocycles. The breathing mode of the heptazine ring was 812 cm^{-1}, and no obvious sulfur peak was found in the SCN spectrum. Regarding ZIF-8, the peaks at 420 cm^{-1} show the stretching of Zn–N bonds because the Zn atoms in ZIF-8 connect with the N atoms of the 2-MI linker during ZIF-8 synthesis. Both the XRD and FT-IR spectra of pure ZIF-8 and ZIF-8 composites are not noticeably shifted, indicating that these nanocomposites are physically bound rather than forming chemical bonds.

The surface morphologies of ZIF-8/GCN and ZIF-8/SCN nanocomposites were obtained using FE-SEM. GCN and SCN show rippled 2D morphologies and paper graphene-like structures. ZIF-8 has a rhombic dodecahedral morphology with an

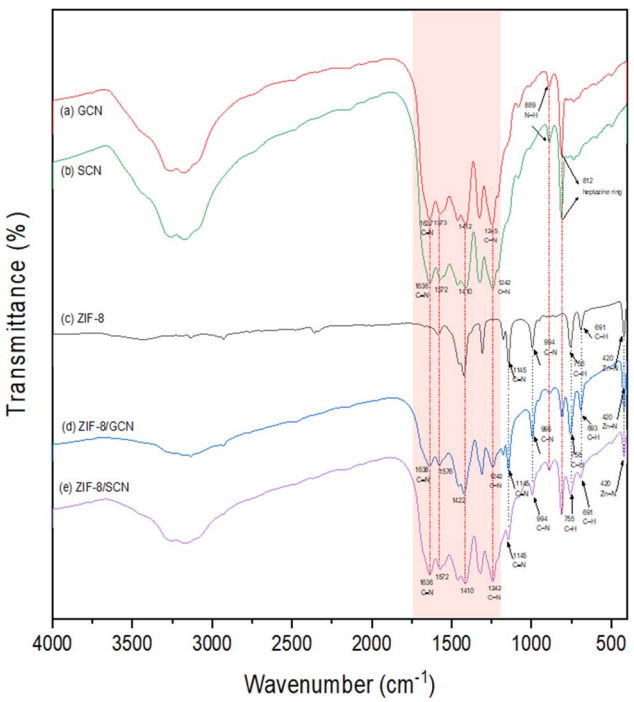

Fig. 2 FT-IR patterns of synthesized (a) GCN, (b) SCN, (c) ZIF-8, (d) ZIF-8/GCN, and (e) ZIF-8/SCN.

average particle size of 300–500 nm (Fig. 3c). The GCN nanosheets act as a support, and rhombic dodecahedral ZIF-8 is deposited on its surface.

Activation energy

The kinetic reactions of the epoxy polymer with different reaction promoters were investigated using DSC at heating rates of 2, 5, 10, and 20 °C min^{-1}. The glass transition temperature (T_g) and the temperature of the maximum degradation rate (T_{peak}) of the epoxy polymers are presented. The obtained data were plotted using Kissinger's equation to calculate the activation energy.[29]

$$-\ln\left(\frac{\theta}{T_{peak}^{2}}\right) = \frac{E_a}{RT_{peak}} - \ln\left(\frac{nAR}{W_m^{n-1}}\right) \quad (1)$$

where θ is the heating rate (K min^{-1}), n is the apparent reaction order, A is the pre-exponential factor, R is the universal gas constant (J K^{-1} mol^{-1}), E_a is the activation energy (kJ mol^{-1}), and W_m is the sample weight at the maximum rate for weight loss. Fig. 4 shows the change in T_{peak} due to the differences in

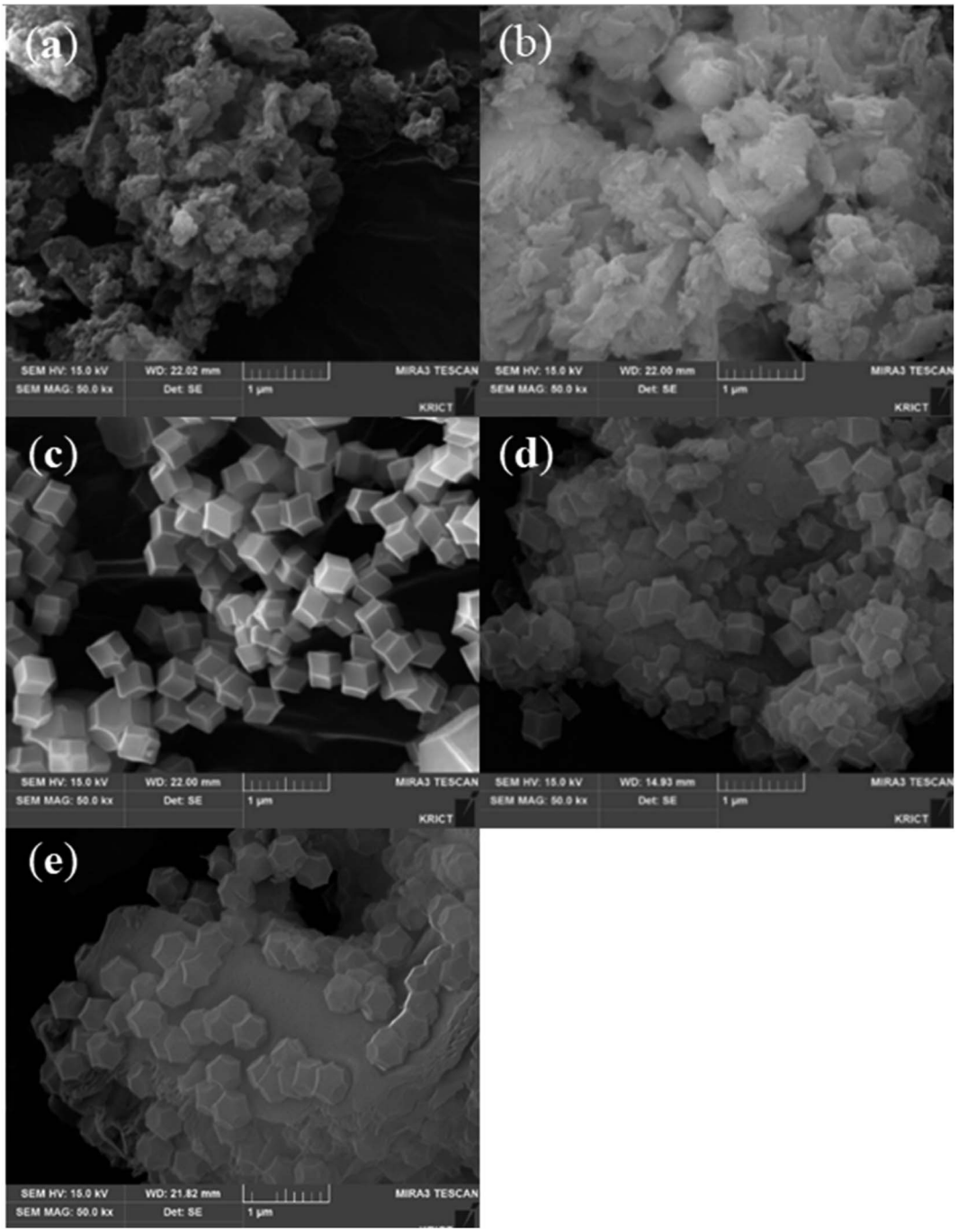

Fig. 3 SEM images of synthesized (a) GCN, (b) SCN, (c) ZIF-8, (d) ZIF-8/GCN, and (e) ZIF-8/SCN.

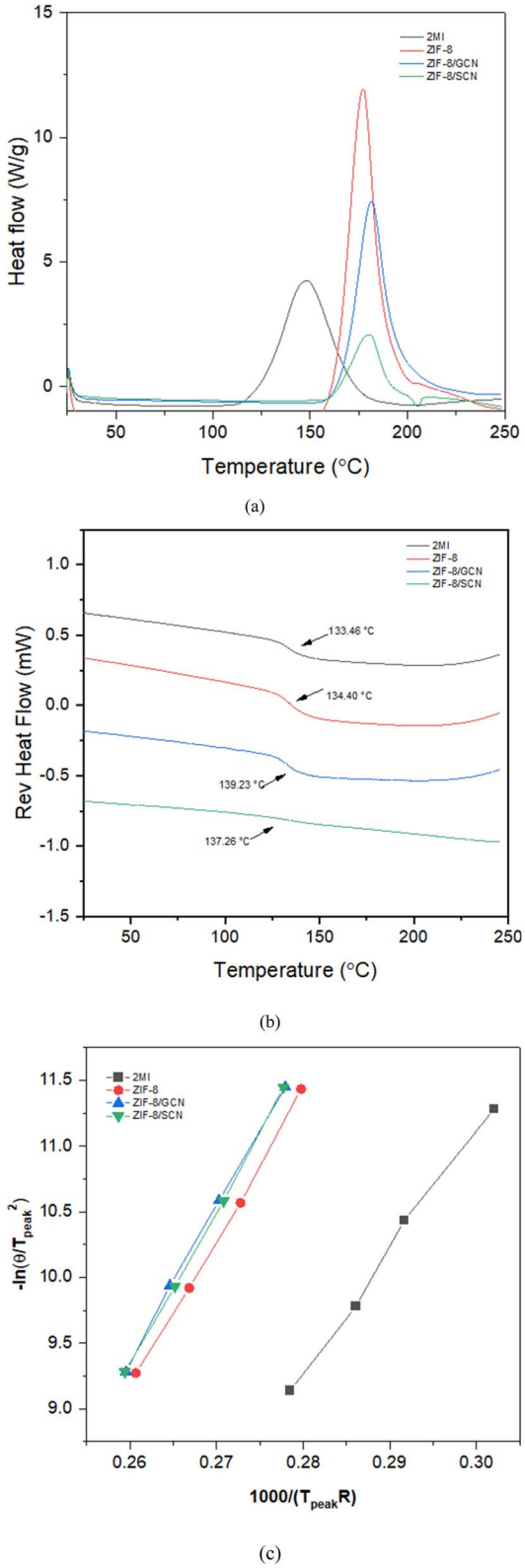

Fig. 4 The DSC plots for epoxy compositions with different promoters: (a) change in T_{peak} (b) glass transition temperature (T_g), and (c) Kissinger plots of activation energy.

Table 2 DSC data for the epoxy compositions

	Heating rate (°C min^{-1})				Activation energy (kJ mol^{-1})
	2	5	10	20	
2-MI	125.21	139.36	147.41	158.87	92.20
ZIF-8	156.94	167.94	177.74	188.41	113.07
ZIF-8/GCN	159.72	172.01	181.55	190.42	117.00
ZIF-8/SCN	160.09	175.13	180.53	190.68	119.79

the heating rates. The epoxy composition with 2-MI has the lowest T_g of 133.36 °C, while the ZIF-8/GCN and ZIF-8/SCN nanocomposites display the highest T_g of 139.23 °C and 137.26 °C, respectively. Fig. 4c displays a straight line with the slope of the activation energy fitted by $-\ln(\theta/T_{peak}^2)$ *versus* $1/RT_{peak}$. The thermal data in Table 2 indicate that there is slight substantial difference in the calculated activation energies for ZIF-8, ZIF-8/

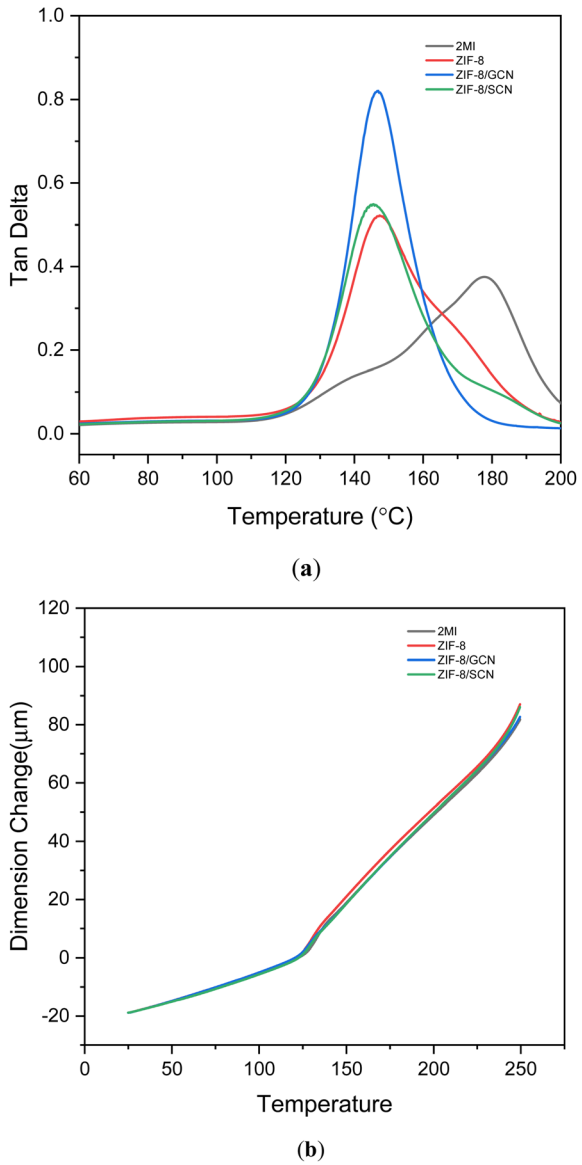

Fig. 5 (a) DMA and (b) TMA data for epoxy compositions with different promoters.

GCN, and ZIF-8/SCN nanocomposites. Activation energy observation showed that ZIF-8 has the function of an epoxy reaction accelerator. However, GCN or SCN, which have tertiary amines in their structures, do not seem to affect the epoxy polymerization reaction rate. This suggests that the tertiary amine of GCN/SCN does not have an open enough structure to interact with the epoxy resin to act as a reaction accelerator.

DMA and TMA

The viscoelastic and thermal properties of each epoxy polymer composition were measured using DMA and TMA. The T_g values derived from the tan δ curves and the CTE values are shown in Fig. 5 and Table 3, respectively. The glass transition temperature (tan δ) of the epoxy compositions with ZIF composites is higher than that of the 2-MI epoxy composition, meaning that the promoters enhance physical crosslinking in the epoxy compositions. CTE values are reported for both parts of the TMA curve: below (70–100 °C) or above the T_g (150–170 °C). The CTE values obtained with different promoters show similar temperatures due to low addition of promoters in the epoxy compositions, respectively.

Mechanical properties of the epoxy compositions

Fig. 6 and Table 4 summarize the mechanical strengths of the epoxy compositions. The epoxy compositions containing ZIF-8, ZIF-8/GCN, and ZIF-8/SCN nanocomposites exhibit higher tensile strengths (20.3%, 29.7%, and 31.4%, respectively) than the epoxy compositions containing 2-MI. The same trend is observed for the impact strength, as shown in Fig. 6c. The flexural strengths of the various composites had no positive impact, as opposed to those of epoxy compositions containing 2-MI. Fig. 6 shows that the impact strength of the epoxy polymers increases from 40.21 to 58.40 J m^{-1} when ZIF-8/SCN nanocomposites are used. The significantly enhanced tensile and impact moduli of the nanocomposites are attributed to the excellent interfacial bonding formed by residual functional groups (–NH_2 or –NH) in GCN between GCN and epoxy. Epoxy ring opening polymerization produces free hydroxyl groups and tertiary amine groups that can lead strong hydrogen bond formation with amine group of GCN or SCN. Additionally, the C═S rigidity bond of SCN supports the slightly stronger strength of SCN composites than GCN composites in terms of tensile and flexural strengths. In addition, the curly structure and large specific surface area of GCN also enhance the mechanical interlocking effect with the matrix.[23,24]

Fracture morphology after impact test

Fig. 7 shows the fracture morphologies of epoxy compositions with different promoters. The scanning electron microscopy (SEM) images of the 2-MI epoxy resins display smooth fracture surfaces. The epoxy resins with different promoters have rougher fracture surfaces than the 2-MI epoxy resins and many wave-like patterns ascribed to the strong interaction between the promoters and epoxy matrix[30–32] are also observed. The external stress is more absorbed on the surface of both GCN or SCN composites in wave-like patterns with crack deflection and aggregation on the surface. Therefore, the wave-like patterns on the surface increase with impact strength, indicating that the synthesized composites enhance the tensile and Izod impact strengths of the epoxy resins.

Table 3 DMA and TMA data for the epoxy compositions

	α_1	α_2	α_2/α_1	T_g (°C, with DMA)
2-MI	66.02	210.7	3.19	138.2
ZIF-8	68.05	217.9	3.20	147.3
ZIF-8/GCN	66.44	211.9	3.18	146.9
ZIF-8/SCN	65.22	214.3	3.28	145.6

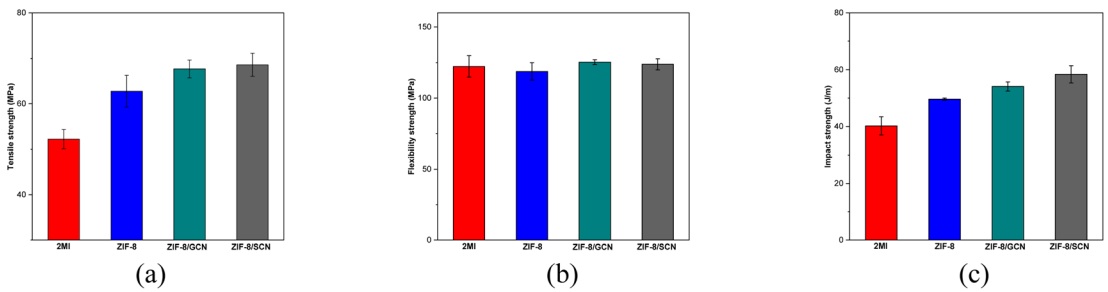

Fig. 6 Mechanical properties of epoxy compositions with different promoters: (a) tensile (MPa), (b) flexural (MPa), and (c) impact (J m^{-1}) strengths.

Table 4 Mechanical properties of epoxy compositions

	2-MI	ZIF-8	ZIF-8/GCN	ZIF-8/SCN
Tensile strength (MPa)	52.19 (±2.13)	62.77 (±3.50)	67.70 (±1.96)	68.58 (±2.5)
Flexure strength (MPa)	122.28 (±7.49)	118.85 (±6.19)	125.37 (±1.70)	123.82 (±3.96)
Impact strength (J m^{-1})	40.21 (±3.19)	49.64 (±0.37)	54.10 (±1.62)	58.40 (±3.06)

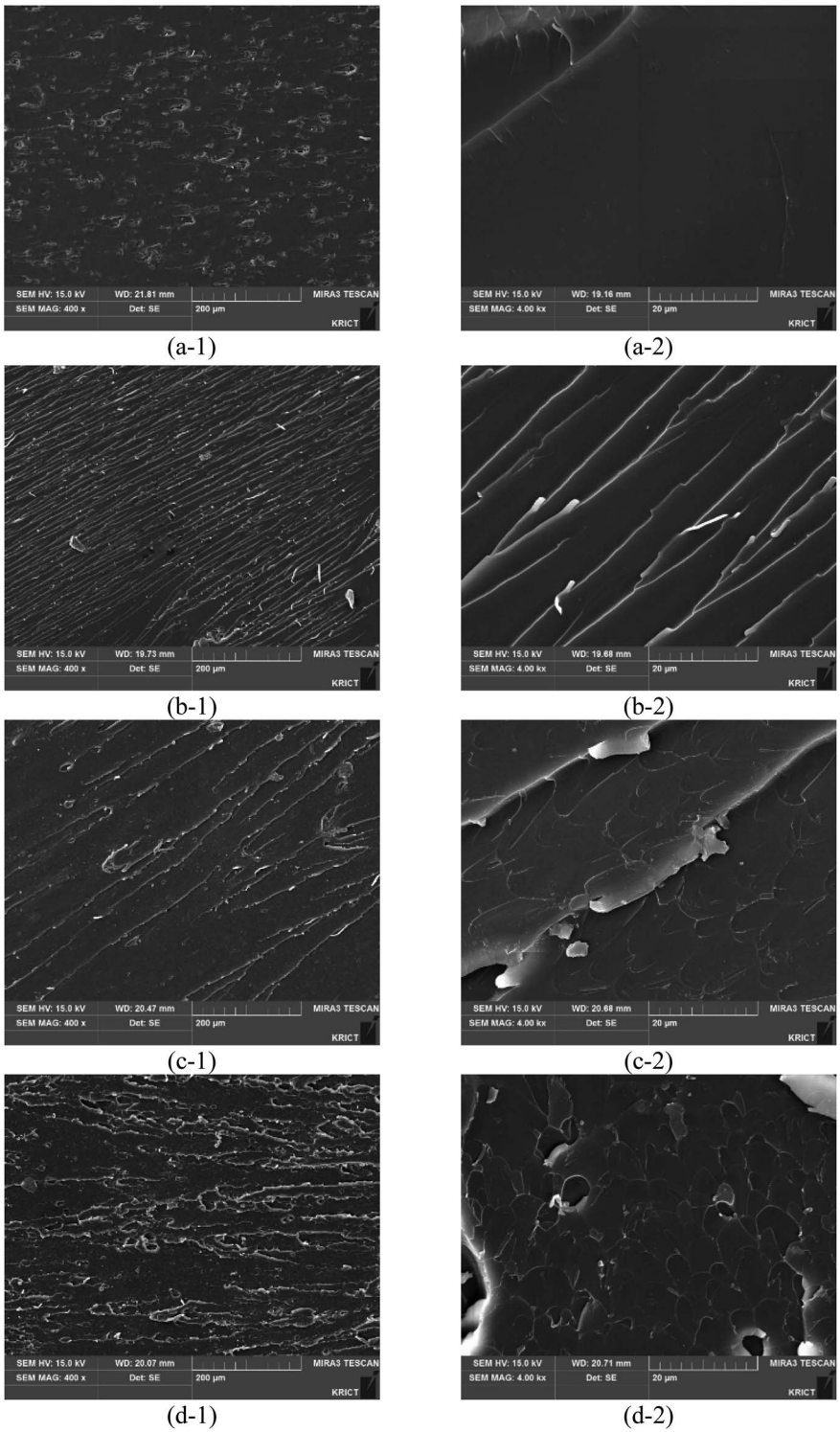

Fig. 7 SEM images of the fractured surfaces of Izod test specimens for different promoters: (a1-a2) 2MI, (b1-b2) ZIF-8, (c1-c2) ZIF-8/GCN, and (d1-d2) ZIF-8/SCN.

Storage stability test

The storage stability of the epoxy compositions was measured by observing the changes in viscosity over time at a constant temperature. Fig. 8 shows the storage stability of the epoxy compositions with different promoters at 40 °C (Fig. 8a) and 60 °C (Fig. 8b). At 40 °C, the viscosity of the 2-MI epoxy resin in the curing system increases with time from 3.57 Pa·s in 1 h to 40.8 Pa·s in 1 day, while at 60 °C, the viscosity increases from 0.57 Pa·s in 1 h to 75 Pa·s in 8 h. However, there is no change in viscosity after the addition of ZIF-8/GCN and ZIF-8/SCN epoxy

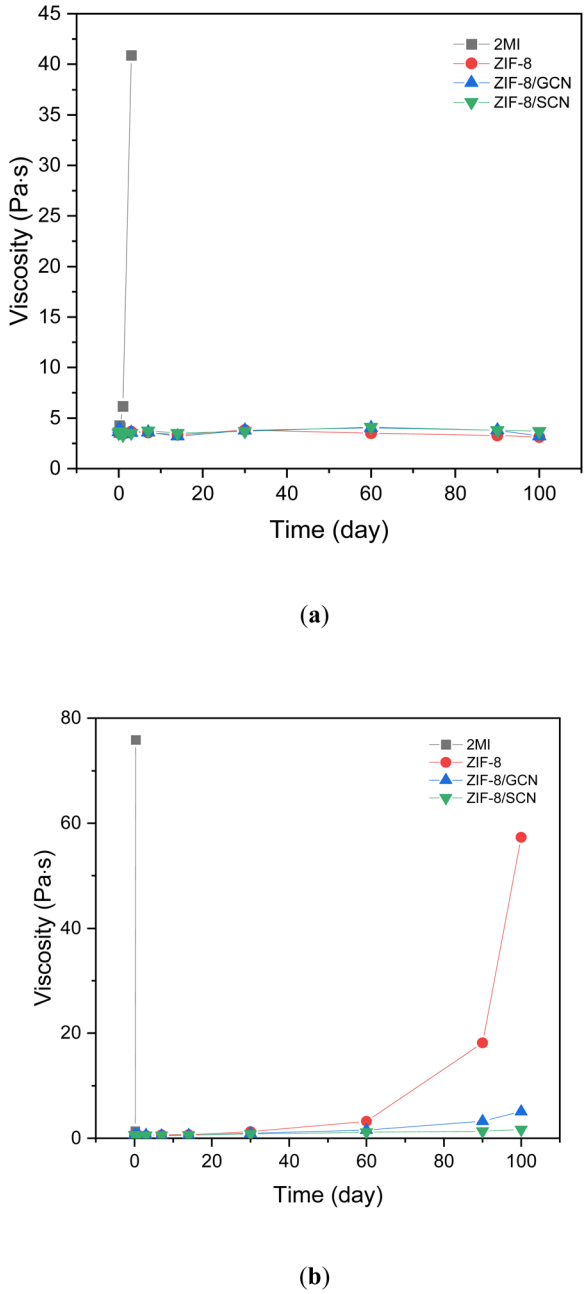

Fig. 8 The plot of change in viscosity over time for different promoters in the curing system at (a) 40 °C and (b) 60 °C.

resins at 40 °C and 60 °C for up to 100 days. This indicates that the addition of ZIF-8/GCN and ZIF-8/SCN reduces the curing reaction rate and increases the effective working life.

Conclusions

The synthesized GCN and SCN nanocomposites acted as promoters. The calculated activated energy of the synthesized nanocomposites was slightly higher than for other promoters using DSC analysis. Additionally, the T_g of epoxy compositions with synthesized promoters was higher than that of other promoters, such as 2-MI. The significant improvements in mechanical properties like tensile and impact strengths were 31.4% and 45.2% higher, respectively, compared with 2-MI epoxy compositions. The wave-like patterns in the fracture images led to the synthesized promoters having improved mechanical properties. From the storage stability tests, both ZIF-8/GCN and ZIF-8/SCN epoxy resins were found to be more suitable for long-term storage than 2-MI epoxy resins. Thus, epoxy compositions with synthesized promoters have the advantage of long-term storage stability and enhanced mechanical properties.

Author contributions

Sugyeong Jeon: methodology, writing – original draft, preparation, formal analysis, and investigation. Hye Jin Kim: methodology, writing – review and editing, and formal analysis. Hyeon-Gook Kim: conceptualization, writing, reviewing, and editing. Meysam Tayebi: formalysis. Seoyoon Yu: investigation. Jong-Hyun Kim: methodology. Bongkuk Seo: conceptualization, writing, reviewing, and editing. Choong-Sun Lim: supervision, conceptualization, writing, review, and editing. Weon Bae Ko: writing, reviewing, and editing.

Conflicts of interest

There are no conflicts to declare.

Acknowledgements

The research received funding from the Technology Innovation Program funded by the Ministry of Trade, Industry & Energy (MOTIE, Korea) under Grant Agreement No. 20011124, TS247-28R and by the KRICT core project funded by the Korea Research Institute of Chemical Technology under Grant Agreement KS2441-10.

References

1 F. L. Jin, X. Li and S. J. Park, *J. Ind. Eng. Chem.*, 2015, **29**, 1–11.
2 A. Wegmann, *Prog. Org. Coat.*, 1997, **32**(1–4), 231–239.
3 T. Dyakonov, Y. Chen, K. Holland, J. Drbohlav, D. Burns, D. Vander Velde and W. T. Stevenson, *Polym. Degrad. Stab.*, 1996, **53**(2), 217–242.
4 T. H. Kim, M. Kim, W. Lee, H. G. Kim, C. S. Lim and B. Seo, *Coatings*, 2019, **9**(5), 319.
5 M. Hesabi, A. Salimi and M. H. Beheshty, *Eur. Polym. J.*, 2019, **112**, 736–748.
6 M. Hesabi, A. Salimi and M. H. Beheshty, *Polym. Test.*, 2017, **59**, 344–354.
7 K. Fryauf, V. Strehmel and M. Fedtke, *Polymer*, 1993, **34**(2), 323–327.
8 M. Hayaty, H. Honarkar and M. H. Beheshty, *Iran. Polym. J.*, 2013, **22**(8), 591–598.
9 L. R. Amirova, O. L. Khamidullin, K. A. Andrianova and L. M. Amirova, *Polym. Bull.*, 2018, **75**(11), 5253–5267.
10 Y. R. Ham, S. H. Kim, Y. J. Shin, D. H. Lee, M. Yang, J. H. Min and J. S. Shin, *J. Ind. Eng. Chem.*, 2010, **16**(4), 556–559.

11 D. Guzmán, X. Ramis, X. Fernández-Francos and A. Serra, *Polymers*, 2015, **7**(4), 680–694.
12 M. R. Kim, T. Kim, H. S. Rye, W. Lee, H. G. Kim, M. I. Kim and C. S. Lim, *J. Mater. Sci.*, 2020, **55**(5), 2068–2076.
13 J. H. Park, H. J. Kim, T. H. Kim, H. G. Kim, B. Seo, C. S. Lim and W. B. Ko, *Appl. Nanosci.*, 2021, **11**(5), 1491–1500.
14 M. Humayun, H. Ullah, A. A. Tahir, A. R. bin Mohd Yusoff, M. A. Mat Teridi, M. K. Nazeeruddin and W. Luo, *Chem. Rec.*, 2021, **21**(7), 1811–1844.
15 W. J. Ong, L. L. Tan, Y. H. Ng, S. T. Yong and S. P. Chai, *Chem. Rev.*, 2016, **116**(12), 7159–7329.
16 C. Hu, Y. C. Chu, Y. R. Lin, H. C. Yang and K. H. Wang, *Polymers*, 2019, **11**(1), 182.
17 H. Dong, X. Guo, C. Yang and Z. Ouyang, *Appl. Catal., B*, 2018, **230**, 65–76.
18 S. Kumar, S. Karthikeyan and A. F. Lee, *Catalysts*, 2018, **8**(2), 74.
19 S. Cao, J. Low, J. Yu and M. Jaroniec, *Adv. Mater.*, 2015, **27**(13), 2150–2176.
20 S. Cao and J. Yu, *J. Phys. Chem. Lett.*, 2014, **5**(12), 2101–2107.
21 H. S. Mohamed, L. Wu, C. F. Li, Z. Y. Hu, J. Liu, Z. Deng and B. L. Su, *ACS Appl. Mater. Interfaces*, 2019, **11**(36), 32957–32968.
22 A. Ghosh, H. Saini, A. Sarkar, P. Guha, A. K. Samantara, R. Thapa and D. K. Goswami, *Appl. Surf. Sci.*, 2021, **556**, 149773.
23 T. Wang, B. Song and L. Wang, *Polymers*, 2020, **12**(1), 76.
24 Y. Shi, S. Jiang, K. Zhou, C. Bao, B. Yu, X. Qian and R. K. Yuen, *ACS Appl. Mater. Interfaces*, 2014, **6**(1), 429–437.
25 Y. Qi, G. Zhu and J. Zheng, *J. Appl. Polym. Sci.*, 2020, **137**(17), 48598.
26 M. Ismael, Y. Wu, D. H. Taffa, P. Bottke and M. Wark, *New J. Chem.*, 2019, **43**(18), 6909–6920.
27 S. Panneri, M. Thomas, P. Ganguly, B. N. Nair, A. P. Mohamed, K. G. K. Warrier and U. S. Hareesh, *Catal. Sci. Technol.*, 2017, **7**(10), 2118–2128.
28 X. Xiao, Y. Wang, Q. Bo, X. Xu and D. Zhang, *Dalton Trans.*, 2020, **49**(24), 8041–8050.
29 T. Kim, S. Kim, D. G. Lee, C. S. Lim and B. Seo, *J. Appl. Polym. Sci.*, 2018, **135**(19), 46233.
30 S. Chhetri, N. C. Adak, P. Samanta, N. C. Murmu, D. Hui, T. Kuila and J. H. Lee, *Compos. B Eng.*, 2018, **143**, 105–112.
31 S. Chhetri, N. C. Adak, P. Samanta, P. K. Mallisetty, N. C. Murmu and T. Kuila, *J. Appl. Polym. Sci.*, 2018, **135**(15), 46124.
32 Y. He, Q. Chen, S. Yang, C. Lu, M. Feng, Y. Jiang and C. Liu, *Composites, Part A*, 2018, **108**, 12–22.